Erratum

Erratum to "Spectroscopic ellipsometry and reflectometry from gratings (Scatterometry) for critical dimension measurement and in situ, real-time process monitoring" [Thin Solid Films 455–456 (2004) 828–836][☆]

Hsu-Ting Huang[1], Fred L. Terry Jr.*

Department of Electrical Engineering & Computer Science, The University of Michigan, 2417F EECS Building, 1301 Beal Ave., Ann Arbor, MI 48109-2122, USA

Abstract

Spectroscopic, specular reflected light measurements (both ellipsometry-SE, and reflectometry-SR) of grating structures have relatively recently been shown to yield very accurate information on the critical dimensions, wall-angles and detailed wall shape of deep submicron features. The technique is often called 'scatterometry' or optical critical dimension (OCD) measurement. This technique has been moved rapidly from initial demonstrations to significant industrial application. In this paper, we will review the development of this technique for in situ and ex situ applications. When applied in situ, this technique opens up exciting new opportunities for studying the evolution of topography in semiconductor fabrication processes and for applying real-time control methods for nanometer level feature size accuracy. We will briefly comment on limitations and challenges for this measurement technique.
© 2004 Elsevier B.V. All rights reserved.

Keywords: Scatterometry; Critical dimension measurement; Process control

1. Introduction

Spectroscopic ellipsometry (SE) and reflectometry (SR) are key thin film measurement techniques for integrated circuit production. However, use of these methods have until recently been limited to case where a defined test area (typically 100×100 μm or larger) of uniform thin films could be defined for measurement. In situ measurements have been largely limited to unpatterned test wafers. At the Second International Conference on Spectroscopic Ellipsometry, H. Maynard and co-workers reported on exciting work on in situ, real-time spectroscopic ellipsometry measurement on Si CMOS structures to control critical gate etches [1]. While very promising, their work was based on the application of coherent field addition of effective area fractions of quasi-uniform thin film regions [2], and ignored diffraction

effects. The strong effects of diffraction from dense, small scale integrated circuit structures causes these approximations to fail in many interesting cases and continued to limit the applications of SE and SR for patterned wafers.

The use of angle-resolved laser scattering from grating structures has been used in many applications for dimensional measurements. The use of this concept for deep submicron metrology was pioneered by J.R. McNeil and co-workers [3]. They termed this measurement 'scatterometry'. While a successful measurement method, this technique requires angle-resolved laser reflectometry and/or ellipsometry measurements over a wide range of angles of incidence and reflection, and is therefore not applicable for in situ applications and is relatively slow for ex situ, in-line applications. This work, however, did clearly illustrate that measurement of specular mode reflected light from defined grating structures could be analyzed with accurate diffraction modeling algorithms to yield dimensional information with sub-wavelength resolution.

Combining these observations, it became clear that the use of fixed angle of incidence SE or SR measurements

---

* Corresponding author. Tel.: +1-734-763-9764; fax: +1-734-763-9324.

E-mail address: fredty@umich.edu (F.L. Terry).

[1] Now with ThermaWave, Inc., Freemont, Ca.

from period structures had strong promise for high speed topography measurements. Several research groups quickly showed that very accuracy measurements could be made with this method [4–6]. In many cases, SE-based scatterometry measurements have proven to be more detailed and more accurate than top-down scanning electron microscopy (critical dimension or CD-SEM) and this method is being rapidly deployed as an in-line process control tool in the Si IC industry [7–9]. Our group has also applied this method in situ in a reactive ion etch system and demonstrated the first experiment in which the evolution of etched structures were monitored and controlled in real-time [10–12].

The emergence of this approach is directly analogous that of conventional thin film ellipsometry when low cost computers enabled the accurate solution of thin film reflection models. Data from complex thin film stacks could be analyzed very rapidly to yield thin film thickness data that compares favorably to cross-sectional transmission electron microscopy. By now applying structures for which the diffraction problem can be numerically solved nearly exactly, we are in the early phases of realizing the advantages of spectroscopic ellipsometry for patterned structures. In this paper, we will review the theory of this approach; show experimental implementation from ex situ and in situ measurements, discuss some of the limitations that are becoming clear, and comment on future challenges.

2. Topography extraction

The method for topography extraction is outlined below:

1. SE or SR information is collected in specular mode on reflection from a sample with a one-dimensional grating. In all of our measurements, the sample is aligned so that the plane of incidence is perpendicular to the lines of the grating.
2. The reflection problem from the grating is modeled using high-accuracy numerical simulation of the Maxwell's equations problem. The rigorous coupled wave analysis (RCWA) method is most commonly employed, [13] but other solution methods have been used [14].
3. The optical dielectric functions of all materials in the lines and any underlying smooth thin films are assumed as known, and are usually obtained by spectroscopic ellipsometry measurements of similarly prepared unpatterned thin films.
4. Either a pattern matching procedure using a large, pre-simulated library of lineshapes or a parameterized non-linear regression procedure is used to find the best fit between theory and experimental reflection data. In our work, we parameterize the shape of the line and use the Levenberg–Marquardt algorithm to optimize the shape parameters.

The RCWA method solves the diffraction problem from a grating with one-dimensional periodicity with arbitrary lineshape by slicing the line into a series of rectangular regions as illustrated in Fig. 1. The grating can be viewed as a one-dimensinal modulation of the dielectric function along the direction of periodicity (x), and, $\varepsilon(x)$ can be expanded as a Fourier series:

$$\varepsilon(x) = \sum_h \varepsilon_h \exp\left(j\frac{2\pi h}{\Lambda}x \right) \tag{1}$$

This expansion is carried out over each segment or slice in the lineshape approximation. The electromagnetic scattering problem can be solved exactly for each complex sinusoidal component at each slice. Using a state space matrix approach, similar to conventional thin film optics, the allowed solutions can be matched at each slice boundary and the complete complex reflectance and transmission of the grating can be computed for each allowed diffraction mode. If the spatial expansion in h is taken over $\pm \infty$ and the structure is sliced into infinitesimally thin regions (infinite number of slices), then in principal this approach results in an exact solution of the diffraction problem. In practice, of course, a finite number of both spatial orders (N) and slices (s) are used to approximate the problem, and care must be exercised to insure that the solution has converged to an adequate approximation. The convergence of the RCWA algorithm for the p-mode (TM) is significantly improved if the algorithm of Ref. [13] is corrected to the formulation proven by Li [15]. Typically, N may be from ∼ 10 to 100 (or more). Larger values are needed for high dielectric function materials (particularly metals) or if the grating period is large compared to the measurement wavelengths. The number of slices, s, is typically 1 to 50 but depends on the shape of the line.

This approach, while conceptually relatively simple, results in large matrix eigenvalue solutions and presents a very significant computational time problem. However, thanks to the advances in both the speed and cost of computers, practical use of this method is now possible. Also, for either spectroscopic or angle resolved calculations,
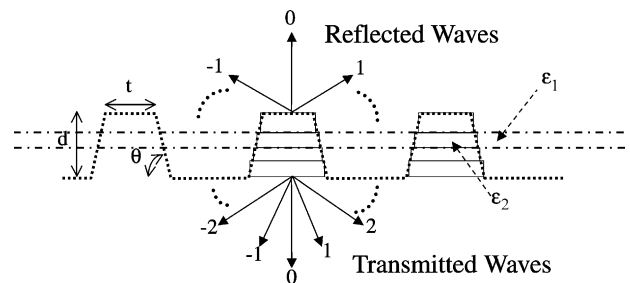

Fig. 1. A schematic illustration of the RCWA method in which the 1-D grating is sliced into a series of rectangular segments. In this figure, ε_1 and ε_2 are the dielectric functions of the material in the grooves and lines of the grating, respectively. Sidewall coatings or any other period variation in the structure can be included in the RCWA calculation through $\varepsilon(x)$.

the problem naturally vectorizes (since each wavelength and/or angle of incidence is a separate computation), and massively parallel computation can be used for real-time calculations [8]. The method has also been extended to two-dimensional arrays (appropriate for contact holes, memory structures, etc.) [16].

3. Ex Situ experiments

We have experimentally investigated a number of ∼ 350 nm structures using wafers with large area 700 nm photoresist gratings on 31.7 nm of SiO$_2$ on a single crystal Si wafer.

The refractive index vs. wavelength of the photoresist was extracted from a similarly processed unpatterned film using spectroscopic ellipsometry at 4 angles of incidence (60, 65, 70, 75°) to reduce the artifacts produced at antireflection points. The period of the grating was verified by measuring the angle of the 1st order diffraction peak as a function of wavelength under an illumination angle of 7°. These data were fit to the classic grating equation:

$$\sin(\theta_D) = \frac{m\lambda}{\Lambda} + \sin(\theta_i) \qquad (2)$$

where Λ is the grating period, λ is the wavelength, θ_i is the angle of incidence, θ_D is the angle of diffraction, and m is the diffracted order. The period can also be included as a regression parameter, but this approach allows very accurate extraction of the period independently of numerical diffraction calculations.

Ex situ spectroscopic ellipsometry measurements were collected using a Sopra GESP-5 rotating polarizer ellipsometer with a photomultiplier/high-resolution scanning monochromator detection system. Data were collected at 7, 63.5, and 73° AOI's in the tracking analyzer mode and will be represented in the α, β format. For this sample, the near-normal configuration proved to be the most sensitive [17], so only that data will be shown in this paper. In other sample cases, AOI's ∼ 60–75° may prove to be advantageous. The choices of 63.5 and 73° AOI's were for comparisons to in situ data collected in our reactive ion etch systems.

The data from both our ex situ and in situ measurements were fit using parameterized geometric models for the lineshape, rigorous coupled wave analysis (RCWA) for the specular scattering calculations, and Levenberg–Marquardt non-linear regression to optimize the fit of the simulations resulting from geometric parameters vs. the measured data.

The capability of this approach to extract detailed topography information is illustrated in Figs. 2–4. Fig. 2 shows a best fit of a trapezoidal approximation (three parameters) for the photoresist line shape. While it reproduces some of the major features in the SE data, it is clearly not a good fit. By increasing the number of parameters in the lineshape description, a much better fit can be obtained as shown in Fig. 3. The
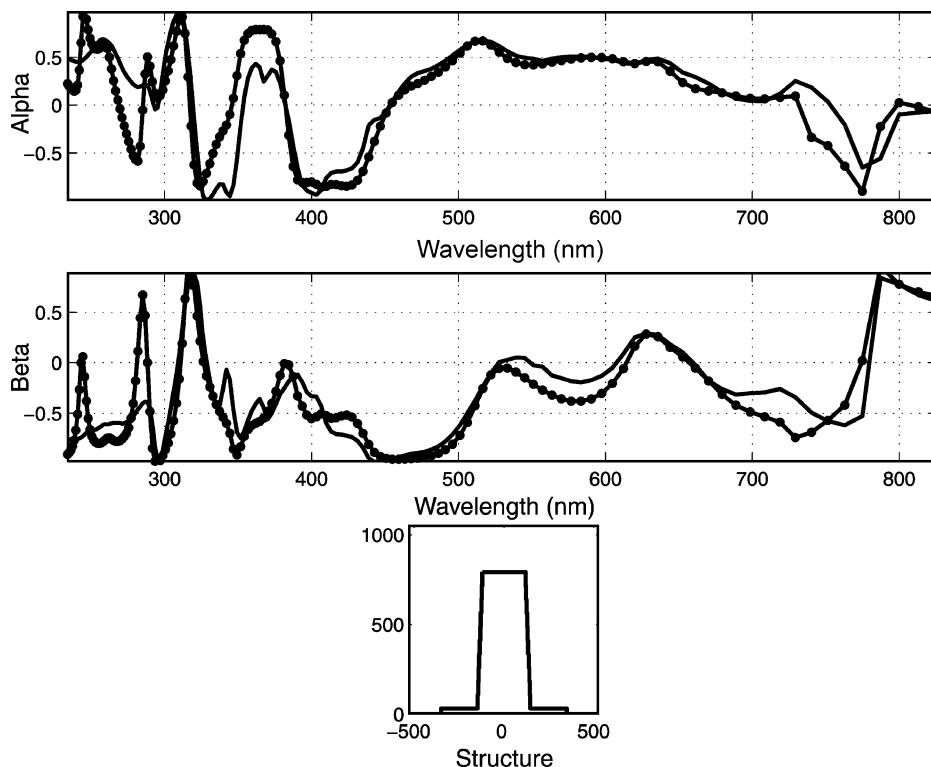

Fig. 2. A best fit of a trapezoidal approximation (three parameters) for the photoresist line shape.
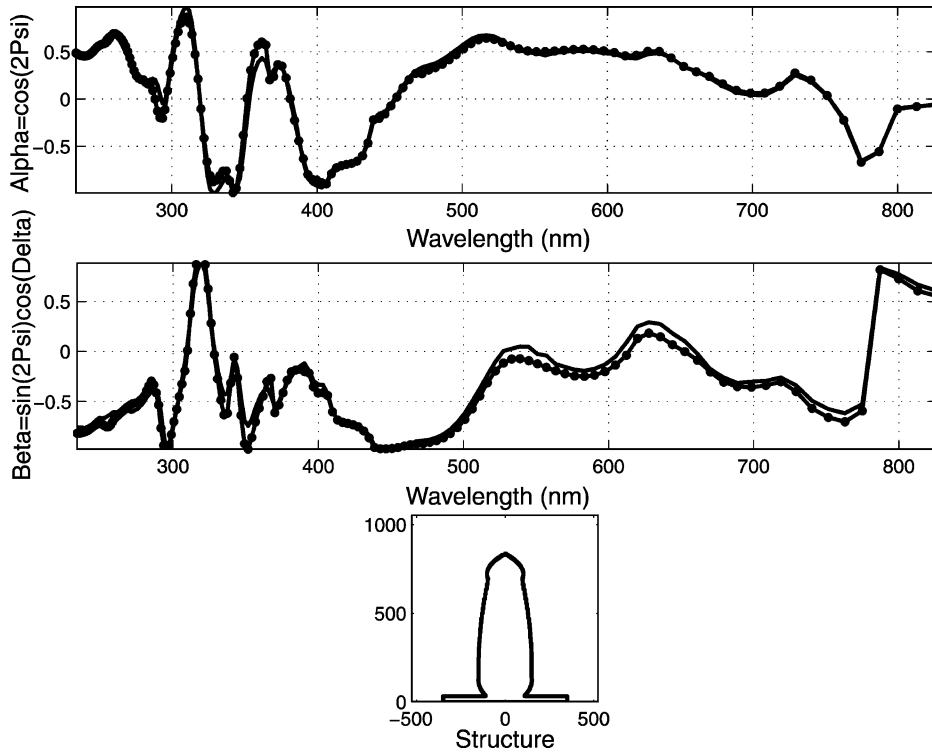
Fig. 3. Best fits to the SE data for the segmented quadratic line shape (nine parameters) fit to the photoresist grating.

parameters used in this fit are shown in Table 1. For each fitted segment j, the width of segment at a given point y measured down from the top of the segment is given by:

$$w(y) = \left[m_{j0} + m_{j1}\left(\frac{y}{h_j}\right) + m_{j1}\left(\frac{y}{h_j}\right)^2 \right] \Lambda \qquad (3)$$

For this fit, we set $m_{10}=0$ for the top curved triangle. This was done since attempts to extract a top width yielded numbers which were essentially zero and which had no statistical significance. The remaining m_{j0}'s were linked to the bottom width of the segment above so that the sidewall structure was a continuous function of y. The approach can be obviously extended to higher order shapes or other functional forms. For this fit, the segmented quadratic results in 9 independent parameters. The standard 95.4% confidence limits for this fit are also shown in the table. All

of the fitted parameter shows confidence limits that are less than the parameters themselves, indicating that all have some statistical validity in the topography extraction. However, when the cross correlation coefficients are examined (Table 2), we see that there is strong coupling between the heights of the main middle segment (h_2) and the height of the lower undercut segment (h_3). Also, we see strong coupling between the slope and the curvature of the main segment (m_{21} and m_{22}). The latter correlation is not too surprising as the middle segment is close to vertical, and thus resolution of the slight curvature is difficult. The $h_2 - h_3$ correlation illustrates the difficulty in clearly resolving the slight undercut. In summary for this point, we have now pushed this data to the limit of statistical merit. Further parameterization could improve the quality of fit, but would not result in topographic parameters for which we could be physically confident. Also, it is quite possible that the residual error in the fit is due to differences between the
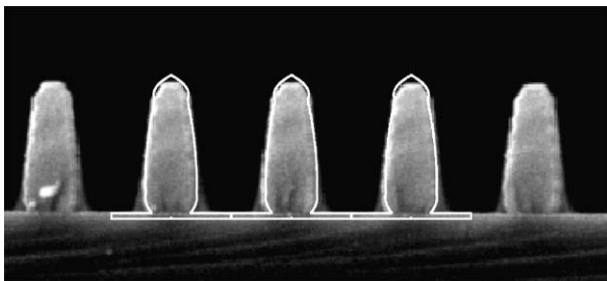

Fig. 4. A cross-sectional SEM photograph of the photoresist grating with the nine parameter quadratic line shape overlaid.

Table 1
Extracted parameters for the fits shown in Figs. 3 and 4

Term	Value	95.4% conf. limit	Units
h1	146.51	4.55	nm
m11	0.7389	0.0097	slope
m12	− 0.4698	0.011	quadratic curvature
h2	545.72	36.05	nm
m21	0.3461	0.0272	slope
m22	− 0.1921	0.0282	quadratic curvature
h3	112.35	34.79	nm
m31	0.0803	0.0529	slope
m32	− 0.1933	0.0659	quadratic curvature

Table 2
Cross-correlation coefficients for the parameter in Table 1. The cross-correlations above 0.9 indicate cause for concern in over-fitting of the data

	h1	m11	m12	h2	m21	m22	h3	m31	m32
h1	1	0.356	− 0.217	− 0.369	− 0.176	0.121	0.267	0.101	0.04
m11	0.356	1	− 0.88	− 0.34	− 0.31	0.354	0.301	− 0.098	0.219
m12	− 0.217	− 0.88	1	0.373	− 0.02	− 0.08	− 0.363	− 0.146	− 0.009
h2	− 0.369	− 0.34	0.373	1	0.512	− 0.527	− 0.993	− 0.369	− 0.108
m21	− 0.176	− 0.31	− 0.02	0.512	1	− 0.981	− 0.493	0.286	− 0.474
m22	0.121	0.354	− 0.08	− 0.527	− 0.981	1	0.517	− 0.31	0.501
h3	0.267	0.301	− 0.363	− 0.993	− 0.493	0.517	1	0.394	0.082
m31	0.101	− 0.098	− 0.146	− 0.369	0.286	− 0.31	0.394	1	− 0.866
m32	0.04	0.219	− 0.009	− 0.108	− 0.474	0.501	0.082	− 0.866	1

actual and assumed photoresist dielectric functions. Besides the normal sources of error in dielectric function estimates, it is possible that the exposure, development, and post-exposure bake processes will affect the lines differently than the unpatterened control sample.

In Fig. 4, we overlap the fits of the segmented quadratic fit on a cross-sectional SEM photo. The extracted optical topography fit was scaled to the photograph by adjusting the size until the period of the simulation matched the period on the SEM. No other scaling was applied. Since the period is very accurately known, we were not dependent on the accuracy of the SEM magnification. As can be seen in Fig. 4, the agreement of the optical fit with the SEM photo is excellent. The nine parameters fit even captures the slight undercut or notching in the photoresist lines. It is also interesting to note that the simple trapezoidal fit, which yielded a relatively poor quality fit to the SE data, captures the average shape of the line well and would yield a good average CD value. In practice, we have found the stated magnification of SEM's to have up to 10% error and (in some cases) that there is distortion (different x and y direction magnifications) in the SEM images. Use of trace-able calibration standards, taking two images for measurement with the fast-scan axis rotated to both the x and y directions, and addressing carefully addressing the known

astigmatic and chromatic aberration effects should reduce these errors; however, it is now well known that accurate metrology with SEM's is much more difficult than high resolution imaging [18].

In a second ex situ example, we etched this pattern into a crystalline Si wafer using reactive ion etching and stripped the photoresist and SiO_2 films. Fitting a simple trapezoidal shape to this data yields an even higher quality fit as illustrated in Fig. 5. The comparison of the SEM and optical extractions of the parameters for this sample are given in Table 3. These cases illustrate that with high quality SE data, well known materials, and good sample uniformity that the extracted critical dimension data is accurate to nanometer levels. Due to the various uncertainties in sample preparation, alignment and instrument resolution, it is difficult or impossible to quantify the measurement accuracy limitations of the optical topography extractions using SEM.

4. In situ measurements and real-time control

In situ measurements and real-time control experiments were conducted using the photoresist grating samples. A Lam 9400 TCP SE poly Si etch system was slightly modified to add ports for ellipsometry. Due to vacuum system constraints, the AOI was 63.5°. Spectroscopic ellipsometry data was collected using a Sopra RTSE (real-time spectroscopic ellipsometer), which is a rotating polarizer SE with a prism spectrometer/CCD array detector for high speed data acquisition. This system allows data collection at a 180 ms sampling rate. The SE measurement itself occurs in 100 ms. This fast data collection rate allows each measurement
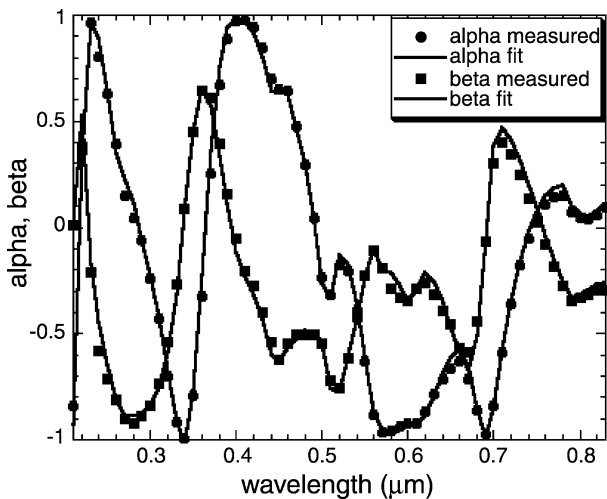

Fig. 5. Measured and fitted SE data for a grating etched into single crystal Si.

Table 3
Parameters from the extraction of topography data from an etched Si grating. The SEM numbers and uncertainties are the best measurements fitted by hand to scale photographs. The SE&RCWA numbers are individual fits to spectroscopic ellipsometry data at 7, 63.5, and 73° angles of incidence. The 7° AOI data and fit are illustrated in Fig. 5

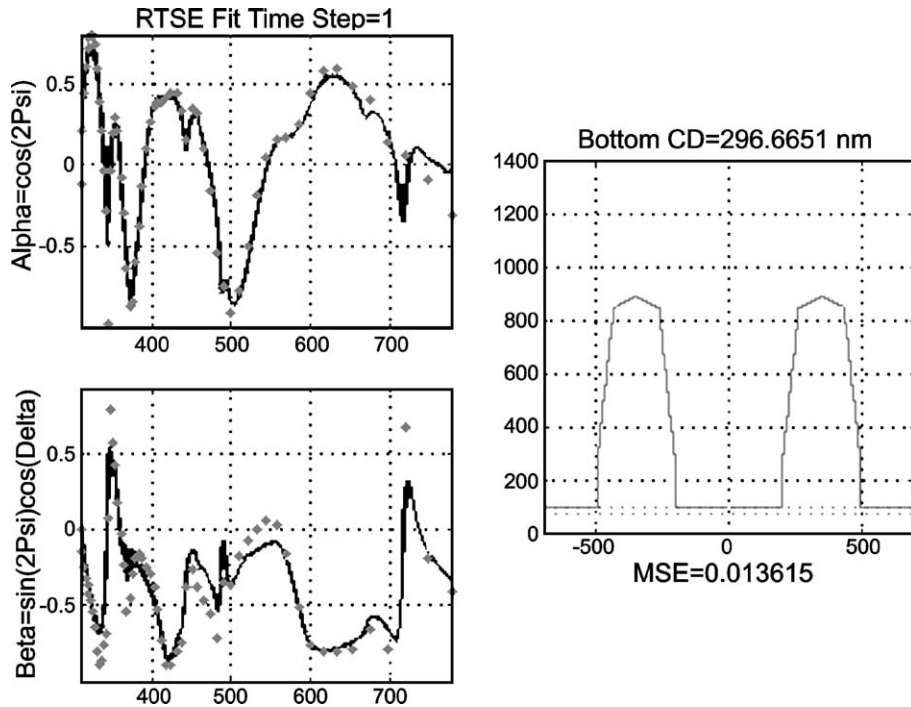| Parameter		CD (nm)	Depth (nm)	Wall angle
SEM		323 ± 5	308 ± 5	84.1° ± 1.4°
SE & RCWA	7°	323 ± 1.7	300 ± 0.4	83.2° ± 0.30°
	63.5°	324 ± 2.8	302 ± 2.7	82.9° ± 0.56°
	73°	321 ± 9.4	302 ± 8.5	82.9° ± 1.8°

Fig. 6. Measured and fitted SE data, and the extracted lineshape taken from in situ ellipsometry data on the original photoresist.

to be treated as a quasi-static snap shot of the sample. The gratings in these tests were rotated so that the plane of incidence was perpendicular to the grating. All of our data was collected with a fixed analyzer position of 45°.

Due to stray light effects, the real-time in situ is somewhat distorted, particularly in regions of rapid variation in $\tan(\psi)$; therefore, fits to the this data would support fewer

statistically significant parameters than the ex situ, scanning monochromator based measurements. We fit photoresist profiles using either a trapezoid on rectangle model (four parameters) or a triangle-trapezoid-rectangle model (five parameters). Even with these limitations, however, it is possible to obtain very good fits to the basic shape of the line and to extract critical dimensions.
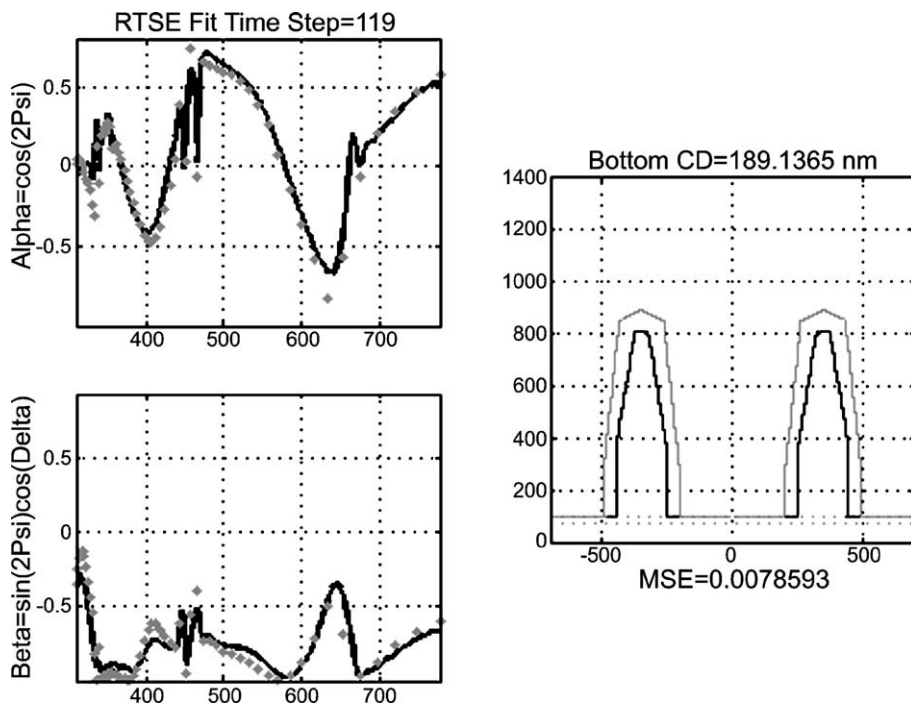

Fig. 7. Measured and fitted SE data, and the extracted lineshape taken from in situ ellipsometry data on the O$_2$ plasma trimmed photoresist.

We used an O_2 plasma to trim-back the photoresist lines. A small library of SE simulations vs. geometries around the expected topography trajectory (based on the trapezoid-rectangle model) was used to determine the coefficients of a convex-hull-based non-linear filtering algorithm (NLF) [11,19]. This NLF is a sort of pattern matching approach with some robustness to noise and experimental data distortions. It allowed rapid topography extraction ($\sim$ 0.25 s on a 600 MHz PIII PC) during the trim-back step. Automatic endpoint was triggered for the desired trim-back to 200 nm bottom CD. This trapezoid on rectangle fit yield a starting condition of 296 nm bottom CD, 169 nm top CD, an 84.2° upper segment sidewall angle and a total line height of 777 nm. The final structure has a 200 nm bottom CD, 71 nm top CD, and 82.1° upper segment sidewall angle, and a total line height of 697 nm. In a later analysis, we used the triangle-trapezoid-rectangle model to extract the most detailed topographic information we could from the logged real-time data. The results of the fit of the original photoresist are shown in Fig. 6 and of the final trimmed photoresist in Fig. 7. Before and after SEM photos with both the trapezoid-rectangle and triangle-trapezoid-rectangle models overlays are shown in Fig. 8. Since the data was collect in real-time, a frame-by-frame animation of the topography evolution process can be produced [20]. The more detailed analysis shows a starting bottom CD of 296.7 ± 9.1 nm and a total photoresist height of 790.0 ± 63.4 nm. After the plasma trim, we obtain a bottom CD of 189.1 ± 29.3 nm and a height of 710.9 ± 67.6 nm (95.4% confidence limits). Better confidence limits would be possible with the improvements in the data quality and/or numerical corrections for the stray light effects. Nevertheless, it is clear from these results that very accurate, real-time control of etched-feature critical dimensions is now possible.
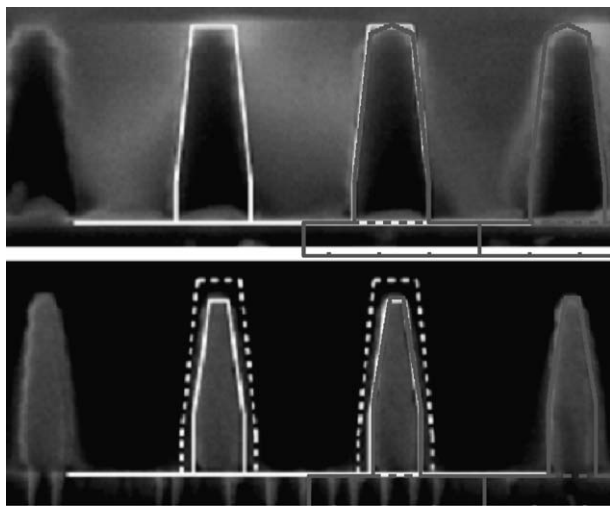

Fig. 8. Original (upper) and O_2 plasma trimmed (lower) SEM photographs of the photoresist grating with both of the optical topography profiles overlaid. The photoresist was trimmed from $\sim$ 300 nm to 200 nm bottom CD.

We have also performed real-time monitoring of the photoresist masked etching of crystalline Si in our Lam 9400 using an HBr/Cl_2 etch chemistry. For brevity, these data will be omitted here but show similar quality levels for CD and etch depth resolution. In one experiment, the SE data yield a Si etch depth of 173.32 ± 0.26 nm and Si CD of 354.62 ± 11.37 nm. Overlays of the SE topography fit and the SEM were of similar quality to photoresist examples we have shown. These SEM do clearly show that Si CD is slightly larger than that of the photoresist mask. This is a well-known effect in this etch chemistry due to sidewall passivation effects from the HBr and possibly redeposited photoresist etch byproducts. This experiment further illustrates the potential of in situ SE measurement to detect CD changes in the critical pattern transfer process and the potential for real-time control to improve process results.

5. Limitations

Our results and those of others have clearly demonstrated that SE-based scatterometry/OCD measurements are capable of extraction of feature shape information that is much better than the Rayleigh criterion. This is, at least in part, due to the fact that we are not performing a general image formation problem. Instead, we are dealing with a situation in which the periodicity of the structure is accurately known (or can be accurately extracted from the optical measurement itself) and we have good assumed values for the optical dielectric functions of the materials being imaged. Thus, we are not using the information contained in the optical signal vs. wavelength to construct a color image, but are rather using this data to obtain the shape. The strong effects of diffraction on this data are then key in the accuracy and detail of these extractions. This situation is directly analogous to determinations of crystal structure using X-ray diffraction, which takes advantage of strong periodicity and knowledge of atomic structure factors.

As features sizes decrease, the capability of scatterometry/OCD also diminishes if the measurement wavelength range is held fixed. In a recent publication, we examined some of these issues using simulations [21]. These results are not fundamentally surprising, since basic theory shows that the strength of scattering decreases as the object size is reduced vs. the wavelength. Our simulations show that useful average CD extractions will be possible for all the gate dimensions envisioned for Si transistors on the Sematech International Technology Roadmap for Semiconductors (ITRS), but that the ability to extract more detailed feature shape information of relevance for sub-100 nm structures will require a move to shorter measurement wavelengths (VUV and perhaps EUV spectral ranges).

As is already the case for the use of SE in very thin gate dielectric measurements, industrial use of the spectro-

scopic scatterometry/OCD techniques will also require very good fundamental accuracy (not merely repeatability) from the measurement instrumentation. This is because at smaller dimensions (CD ≪ λ_{min}), there is no significant structural difference between the SE data for different lineshapes with the same average CD. This is made clear by comparing derivatives of the SE spectra from different simulations (analogous to looking for critical point changes in bulk dielectric function data). For a ∼ 40 nm CD photoresist line on a grating with a 90 nm period, there are small resolvable differences between a rectangular profile and scaled complex profile (similar in shape to our 350 nm lines); however, the maximum differences in (α,β) are ∼ 0.05 and there is no significant difference in the derivative spectra. Thus, near-term Si IC production requirements will push the accuracy of SE instrumentation in these applications.

A second limitation of this method is for very thin structures. Analogously with the problem of dielectric function extraction from very thin uniform films, if the grating is very thin the ability to get even average CD data is poor. This will probably not become a serious issue in wafer-to-wafer process control applications, but this basic limitation must be remembered in real-time monitoring and control applications.

6. Conclusions and discussion

The emerging capability of very high accuracy diffraction calculations allows us to obtain the same quality and types of information in lateral dimensions from spectroscopic ellipsometry that we have previously been accustomed to from uniform thin film measurements. The spectroscopic scatterometry/OCD approach has quickly become a commercially important measurement technology for the Si IC industry. The capabilities offered for studying the chemistry and physics of patterning processes as well as to control these processes is just beginning to be explored. Significant challenges lay ahead for instrumentation and measurement methods for the measurement of structures in the nanoelectronics era. Additional possibilities exist for applications in both semiconductors and other areas if more methods that are practical are developed for diffraction simulations from non-periodic structures (such as those posed by a real product-level IC's). Measurement of single lines or very sparse line arrays would be strong interest to the IC community, but would also potentially of interest in chemistry, biology, nanotube research, and other areas. This would require both more practical diffraction simulation tools and, perhaps more importantly, measurement instrumentation and methodology that would allow adequate signal-noise-ratios for these sparse structures. For the measurement science community, it will be important for us to better understand at a quantitative level the limitations in the accuracy of these methods.

References

[1] H.L. Maynard, N. Layadi, J.T.C. Lee, Thin Solid Films 313–314 (1998) 398.
[2] P.A. Heimann, J. Electrochem. Soc. 132 (1985) 2003.
[3] S.A. Coulombe, A.B.K. Minhas, C.J. Raymond, S.S.H. Naqvi, J.R. McNeil, J. Vac. Sci. Techn. B16 (1998) 80.
[4] M.E. Lee, C. Galarza, W. Kong, W. Sun, F.L. Terry Jr., Characterization and Metrology for ULSI Technology. 1998 International Conference. 23-27 March 1998, Gaithersburg, MD, USA, AIP Conf. Proc. 449 (1998) 331.
[5] N. Xinhui, N. Jakatdar, N. Junwei-Bao, C.J. Spanos, IEEE Trans. Semic. Manuf. 14 (2001) 97.
[6] E.W. Conrad, D.P. Paul, U.S. Patent 5963329, 5 October, 1999.
[7] J. Allgair, P. Herrera, Microlithography World 11 (2002) 12.
[8] J.L. Opsal, H. Chu, Y. Wen, Y.C. Chang, G. Li, SPIE Conference on Metrology, Inspection, and Process Control for Microlithography XVI, Santa Clara, CA, 4–7 March, 2002, SPIE Conf. Proc. 4689, p. 163.
[9] V.A. Ukraintsev, M. Kulkarni, C. Baum, K. Kirmse, M. Guevremont, S. Lakkapragada, K.N. Bhatia, P.P. Herrera, U.K. Whitney, SPIE Conference on Metrology, Inspection, and Process Control for Microlithography XVI, Santa Clara, CA, 4–7 March, 2002, SPIE Conf. Proc. 4689, p. 189.
[10] H.-T. Huang, J.-W. Lee, B.S. Stutzman, P. Klimecky, C. Garvin, P.P. Khargonekar, F.L. Terry Jr., SEMATECH AEC/APC Symposium, Lake Tahoe, NV., 25–28 September, 2000.
[11] H.-T. Huang, J.-W. Lee, B.S. Stutzman, P. Klimecky, P.P. Khargonekar, F.L. Terry Jr., SEMATECH AEC/APC Symposium XIII, Banff, Alberta, Canada, 6–11 October, 2001.
[12] B.S. Stutzman, H.-T. Huang, F.L. Terry Jr., J. Vac. Sci. Techn. B18 (2000) 2785.
[13] M.G. Moharam, D.A. Pommet, E.B. Grann, T.K. Gaylord, J. Opt. Soc. Am. A 12 (1995) 1077.
[14] M.-E. Lee, Ph.D. dissertation, Univesity of Michigan/Dept of EECS, 1999.
[15] L. Li, J. Opt. Soc. Am. A13 (1996) 1870.
[16] J. Opsal, H. Chu, Y. Wen, G. Li, SPIE Conference on Metrology, Inspection, and Process Control for Microlithography XVI, Santa Clara, CA, 24–27 Feb, 2003, SPIE Conf. Proc. 5038, 597.
[17] H.-T. Huang, W. Kong, F.L. Terry Jr., Appl. Phys. Lett 78 (2001) 3983.
[18] D.C. Joy, B.G. Frost, Characterization and Metrology for ULSI Technology. 2000 International Conference. 26–29 June 2000; Gaithersburg, MD, USA, AIP Conf. Proceedings 550, 561.
[19] J.-W. Lee, P.P. Khargonekar, Proceedings of the 40th IEEE Conference on Decision and Control, vol. 3, 2001, p. 2125.
[20] Animated movies from RTSE data can be found on the author's web site www.eecs.umich.edu/ ∼ fredty.
[21] F.L. Terry Jr., SPIE Conference on Metrology, Inspection, and Process Control for Microlithography XVI, Santa Clara, CA, 24–27 Feb, 2003, SPIE Conf. Proc. 5038, p. 547.